




## Single-state or low-lying-states dominance mechanism of $2\nu\beta\beta$ -decay nuclear matrix elements

W. L. Lv (吕万里) <sup>1</sup>, Y. F. Niu (牛一斐) <sup>1,\*</sup>, D. L. Fang (房栋梁) <sup>2,3</sup> and C. L. Bai (白春林)<sup>4</sup>

<sup>1</sup>*School of Nuclear Science and Technology, Lanzhou University, Lanzhou 730000, China*

<sup>2</sup>*Institute of Modern Physics, Chinese Academy of Sciences, Lanzhou 730000, China*

<sup>3</sup>*School of Nuclear Science and Technology, University of Chinese Academy of Sciences, Beijing 100049, China*

<sup>4</sup>*Department of Physics, Science, and Technology, Sichuan University, Chengdu 610065, China*



(Received 28 December 2021; accepted 19 April 2022; published 29 April 2022)

The  $2\nu\beta\beta$ -decay nuclear matrix elements (NMEs) for 11 nuclei are studied with the self-consistent quasi-particle random phase approximation (QRPA) based on the Skyrme Hartree-Fock-Bogoliubov (Skyrme HFB) model. As a common feature pointed out by Šimkovic, Smetana, and Vogel [*Phys. Rev. C* **98**, 064325 (2018)], negative contributions in the running sums of NMEs are found, and play important roles in the fulfillment of the single-state dominance or low-lying-states dominance hypothesis. By comparing the results of the QRPA model and the quasiparticle Tamm-Dancoff approximation (QTDA) model, we find that the negative contributions are due to the enhanced ground-state correlations, which are brought by the backward amplitude in the QRPA model and tuned by strong isoscalar pairing interaction. The enhancement of ground-state correlations will change the signs of  $GT^+$  (Gamow-Teller) transition amplitudes of higher-lying states and leads to the negative contributions in the running sum.

DOI: [10.1103/PhysRevC.105.044331](https://doi.org/10.1103/PhysRevC.105.044331)

### I. INTRODUCTION

Double- $\beta$  ( $\beta\beta$ ) decay is a rare transition process between nuclei  $(A, Z)$  and  $(A, Z + 2)$ . There may exist two modes of this decay. One is the two-neutrino  $\beta\beta$  ( $2\nu\beta\beta$ ) decay with the emission of two antineutrinos. As a second-order weak process, it was first suggested by Mayer [1] and was first observed for  $^{82}\text{Se}$  [2] in the 1980s and for another ten different nuclei later [3]. The other mode is the so-called neutrinoless  $\beta\beta$  ( $0\nu\beta\beta$ ) decay, which is a lepton-number-violating nuclear process and occurs only if neutrinos are their own antiparticles, i.e., the Majorana particles [4,5].  $0\nu\beta\beta$  decay is the only practical way to determine whether neutrinos are Majorana particles and is helpful to address the questions of the absolute neutrino mass scale and the neutrino mass hierarchy, provided that the corresponding nuclear matrix elements (NMEs)  $M^{0\nu}$  are calculated exactly [6–10]. However, the deviations of  $M^{0\nu}$  from different nuclear models vary up to a factor of around 3 (cf. Fig. 26 in Ref. [10]). The main reason of such a divergence stems from the difference of nuclear many-body wave functions obtained from different nuclear models. While  $0\nu\beta\beta$  decay is related to the underlying new physics,  $2\nu\beta\beta$  decay is free from the unknown neutrino properties. Also the corresponding lepton phase-space factor has been calculated with high precision [11,12]. Therefore, the NME of  $2\nu\beta\beta$  decay,  $M^{2\nu}$ , provides a test ground for nuclear structure calculations.

As a second-order weak process, the  $M^{2\nu}$  of  $2\nu\beta\beta$  decay involves a summation over all the virtual intermediate states of the nucleus  $(A, Z + 1)$ , which connects the initial nucleus

$(A, Z)$  and final nucleus  $(A, Z + 2)$  by the  $\beta$ -decay like transitions. Because of isospin symmetry, the Fermi transition is highly suppressed so that only the NME of Gamow-Teller (GT) transition  $M_{\text{GT}}^{2\nu}$  is considered in the calculations. In 1984, Abad proposed the single-state dominance (SSD) hypothesis, which states that the  $M_{\text{GT}}^{2\nu}$  is dominated by the virtual transitions through the first  $1^+$  state of the intermediate nucleus  $(A, Z + 1)$  [13]. It can be extended to the more relaxed low-lying-states dominance (LLD) hypothesis [14]. By analyzing the energy distribution of the emitted electrons, the evidence of SSD for  $^{82}\text{Se}$  and  $^{100}\text{Mo}$  has been found in CUPID [15,16] and NEMO-3 [17] experiments. The mechanism of SSD (LLD) could be either no contributions from highly lying  $1^+$  states or the cancellations among them [18–23]. The running sum, namely, the cumulative contribution from the intermediate states, of  $M_{\text{GT}}^{2\nu}$  is a useful tool in the study of SSD and LLD hypotheses [24]. It has been found that in the running sums, calculated by the quasiparticle random phase approximation (QRPA) [23] or the nuclear shell model with a spin-orbit complete model space [25], the contributions are positive at first and then become negative from states lying around 6–10 MeV. Thus, the appearance of the negative contributions seems to be a universal phenomenon [23]. And such negative contributions could lead to the cancellations among the higher-lying  $1^+$  states and consequently the fulfillment of the SSD or LLD hypothesis. However, the underlying reason for the emergence of such negative contributions still needs investigation.

In the QRPA model, the suppression of  $M_{\text{GT}}^{2\nu}$  is closely related to the isoscalar (IS) pairing, as first identified by Vogel and Zirnbauer in 1986 [26]. By considering the particle-particle interaction, mostly the IS pairing [27], in the QRPA

\* niuyf@lzu.edu.cn

treatment of  $2\nu\beta\beta$  decay, the highly suppressed  $M_{\text{GT}}^{2\nu}$  of  $^{130}\text{Te}$  was successfully reproduced [26]. They also found that, as a function of the strength of IS pairing, the  $M_{\text{GT}}^{2\nu}$  of  $^{130}\text{Te}$  monotonically decreases and passes through zero, which was later found to be a common feature in many nuclei in subsequent studies [6,27–32]. Such a suppression of  $M_{\text{GT}}^{2\nu}$  when increasing IS pairing strength is found to be related to the restoration of the Wigner's spin-isospin SU(4) symmetry [26,27,30,33,34]. On the other hand, the ground-state correlations introduced by the backward amplitude in QRPA calculations compared to those of the quasiparticle-Tamm-Dancoff approximation (QTDA) model were also shown to have the suppression effects on the NME [28].

The aim of this paper is to understand the mechanism of cancellation among higher-lying  $1^+$  states that makes SSD and LLD hypotheses valid. Inspired by the previous works on the suppression of the NME, particular attention will be paid to the effects of IS pairing as well as ground-state correlations on the negative contributions in the running sums of  $M_{\text{GT}}^{2\nu}$ . During the past few decades, different nuclear models have been used in the study of  $M_{\text{GT}}^{2\nu}$  (see Refs. [6–10] for a review), such as the nuclear shell model [25,35–39], QRPA model [23,24,26–32,37,40–46], projected Hartree-Fock-Bogoliubov model [47–51], and interacting boson model [52,53]. One of the models which can avoid the closure approximation is the QRPA. The closure approximation is not appropriate for  $2\nu\beta\beta$  decay [7]. To study the running sum of the NME, one must go beyond this approximation.

In this work, we adopt the spherical QRPA approach based on the Skyrme Hartree-Fock-Bogoliubov model (Skyrme HFB + QRPA) to systematically study the  $M_{\text{GT}}^{2\nu}$  of 11 nuclei with experimental NMEs. We focus on the cancellation among higher-lying  $1^+$  states in the running sum of  $M_{\text{GT}}^{2\nu}$  that leads to the fulfillment of SSD or LLD hypothesis. Compared to the QTDA model, the QRPA model introduces more ground-state correlations through the backward amplitude  $Y_{\pi\nu}$ . We will study the importance of these ground-state correlations. Their effects, entangled with the IS pairing, on the negative contributions of the running sums for  $M_{\text{GT}}^{2\nu}$  are analyzed in detail. The QRPA model as well as the formalism for calculating the  $M_{\text{GT}}^{2\nu}$  are presented in Sec. II. Numerical details of our Skyrme HFB + QRPA calculations are presented in Sec. III. Section IV contains the results and discussions. The summary is given in Sec. V.

## II. FORMALISM

### A. Quasiparticle random phase approximation

We first perform the Skyrme HFB calculation, the formalism of which can be found in Refs. [54–56]. Then with the obtained canonical single-particle wave functions and occupation amplitudes, the QRPA equations for the state  $|nJ^P\rangle$  with angular momentum  $J$  and parity  $P$  can be constructed in the angular momentum coupled form

$$\begin{pmatrix} A & B \\ -B & -A \end{pmatrix} \begin{pmatrix} X^{nJ^P} \\ Y^{nJ^P} \end{pmatrix} = \Omega^{nJ^P} \begin{pmatrix} X^{nJ^P} \\ Y^{nJ^P} \end{pmatrix}, \quad (1)$$

where  $X^{nJ^P}$  and  $Y^{nJ^P}$  are respectively the forward and backward amplitudes, and  $\Omega^{nJ^P}$  are the energy eigenvalues. In the charge-exchange case, using the canonical basis the matrices  $A$  and  $B$  can be expressed as

$$\begin{aligned} A_{\pi\nu,\pi'\nu'} &= (u_{\pi}u_{\pi'}h_{\pi\pi'} - v_{\pi}v_{\pi'}h_{\bar{\pi}\bar{\pi}}^T \\ &\quad - u_{\pi}v_{\pi'}\Delta_{\pi\bar{\pi}} + v_{\pi}u_{\pi'}\Delta_{\bar{\pi}\pi}^*)\delta_{\nu\nu'} \\ &\quad + (u_{\nu}u_{\nu'}h_{\nu\nu'} - v_{\nu}v_{\nu'}h_{\bar{\nu}\bar{\nu}}^T \\ &\quad - u_{\nu}v_{\nu'}\Delta_{\nu\bar{\nu}} + v_{\nu}u_{\nu'}\Delta_{\bar{\nu}\nu}^*)\delta_{\pi\pi'} \\ &\quad + (u_{\pi}v_{\nu}u_{\pi'}v_{\nu'} + v_{\pi}u_{\nu}v_{\pi'}u_{\nu'})\langle\pi\nu'|V|\nu\pi'\rangle_J^{\text{ph}} \\ &\quad + (u_{\pi}u_{\nu}u_{\pi'}u_{\nu'} + v_{\pi}v_{\nu}v_{\pi'}v_{\nu'})\langle\pi\nu|V|\pi'\nu'\rangle_J^{\text{pp}}, \end{aligned} \quad (2a)$$

$$\begin{aligned} B_{\pi\nu,\pi'\nu'} &= (v_{\pi}u_{\nu}u_{\pi'}v_{\nu'} + u_{\pi}v_{\nu}v_{\pi'}u_{\nu'})\langle\pi\nu'|V|\nu\pi'\rangle_J^{\text{ph}} \\ &\quad - (v_{\pi}v_{\nu}u_{\pi'}u_{\nu'} + u_{\pi}u_{\nu}v_{\pi'}v_{\nu'})\langle\pi\nu|V|\pi'\nu'\rangle_J^{\text{pp}}, \end{aligned} \quad (2b)$$

where  $u$  and  $v$  are the occupation amplitudes.  $h$  and  $\Delta$  are respectively the single-particle Hamiltonian and pairing field.  $|\pi\rangle$  and  $|\nu\rangle$  represent respectively the proton and neutron canonical states. Their time reversal states are denoted as  $|\bar{\pi}\rangle$  and  $|\bar{\nu}\rangle$ . The residual interactions  $V$  are divided into the particle-hole (ph) channel and the particle-particle (pp) channel respectively. For the ph channel, the same Skyrme interaction used in the HFB calculation is adopted. For the pp channel, namely the proton-neutron pairing, the density-dependent  $\delta$  force is used, which can be further divided into the isovector (IV) part

$$V_{T=1}(\mathbf{r}_1, \mathbf{r}_2) = f_{\text{IV}} \left( t'_{0\pi\nu} + \frac{t'_{3\pi\nu}}{6} \rho(\mathbf{r}) \right) \delta(\mathbf{r}_1 - \mathbf{r}_2) \frac{1 - \hat{P}_{\sigma}}{2} \quad (3)$$

and the isoscalar (IS) part

$$V_{T=0}(\mathbf{r}_1, \mathbf{r}_2) = f_{\text{IS}} \left( t'_{0\pi\nu} + \frac{t'_{3\pi\nu}}{6} \rho(\mathbf{r}) \right) \delta(\mathbf{r}_1 - \mathbf{r}_2) \frac{1 + \hat{P}_{\sigma}}{2}, \quad (4)$$

where  $\mathbf{r} = (\mathbf{r}_1 + \mathbf{r}_2)/2$ , and  $\hat{P}_{\sigma}$  is the spin-exchange operator. Parameters  $t'_{0\pi\nu}$  and  $t'_{3\pi\nu}$  are set as the average of the proton-proton and neutron-neutron pairing strengths, which are determined from the Skyrme HFB calculations to reproduce the proton and neutron pairing gaps from the five-point formula of experimental binding energies respectively. Then in QRPA calculations,  $f_{\text{IV}}$  is fixed to make the Fermi  $2\nu\beta\beta$  matrix element vanish as it should, due to the different isospin quantum numbers of the mother nucleus ( $T$ ) and daughter nucleus ( $T - 2$ ). The strength of isoscalar proton-neutron pairing  $f_{\text{IS}}$  is not well constrained [57]; it is usually fixed through fitting the experimental NME. We note that the isovector proton-neutron pairing  $V_{T=1}$  does not affect the Gamow-Teller  $2\nu\beta\beta$  matrix element  $M_{\text{GT}}^{2\nu}$  [32].

### B. $2\nu\beta\beta$ -decay nuclear matrix element

For the  $2\nu\beta\beta$  decay, due to isospin symmetry, the NME is dominated by GT transitions,  $M_{\text{GT}}^{2\nu}$ . For the ground-state-to-

ground-state  $2\nu\beta\beta$  decay,  $M_{\text{GT}}^{2\nu}$  can be expressed as

$$M_{\text{GT}}^{2\nu} = \sum_{n_i n_f} \frac{\langle 0_{\text{g.s.}}^{+(f)} | | \hat{O}_{\text{GT}}^- | | 1_{n_f}^+ \rangle \langle 1_{n_f}^+ | 1_{n_i}^+ \rangle \langle 1_{n_i}^+ | | \hat{O}_{\text{GT}}^- | | 0_{\text{g.s.}}^{+(i)} \rangle}{E_{\text{int.}}(n_i, n_f) + M_{\text{int.}} - (M_f + M_i)/2}, \quad (5)$$

where  $\langle 1_{n_i}^+ | | \hat{O}_{\text{GT}}^- | | 0_{\text{g.s.}}^{+(i)} \rangle$  is the  $\text{GT}^-$  transition amplitude of the initial nucleus to the intermediate nucleus. It can be obtained from the QRPA model as

$$\begin{aligned} \langle 1_{n_i}^+ | | \hat{O}_{\text{GT}}^- | | 0_{\text{g.s.}}^{+(i)} \rangle &= \sum_{\pi_i \nu_i} -\langle j_{\pi_i} | | \hat{O}_{\text{GT}}^- | | j_{\nu_i} \rangle \\ &\times (X_{\pi_i \nu_i}^{n_i} u_{\pi_i} v_{\nu_i} + Y_{\pi_i \nu_i}^{n_i} v_{\pi_i} u_{\nu_i}). \end{aligned} \quad (6)$$

And the transition from the intermediate states to the final nucleus  $\langle 0_{\text{g.s.}}^{+(f)} | | \hat{O}_{\text{GT}}^- | | 1_{n_f}^+ \rangle$  can be expressed as

$$\begin{aligned} \langle 0_{\text{g.s.}}^{+(f)} | | \hat{O}_{\text{GT}}^- | | 1_{n_f}^+ \rangle &= -\langle 1_{n_f}^+ | | \hat{O}_{\text{GT}}^+ | | 0_{\text{g.s.}}^{+(f)} \rangle \\ &= \sum_{\pi_f \nu_f} -\langle j_{\pi_f} | | \hat{O}_{\text{GT}}^+ | | j_{\nu_f} \rangle \\ &\times (X_{\pi_f \nu_f}^{n_f} v_{\pi_f} u_{\nu_f} + Y_{\pi_f \nu_f}^{n_f} u_{\pi_f} v_{\nu_f}). \end{aligned} \quad (7)$$

The overlap factor between the intermediate states constructed from the initial and final nuclei  $\langle 1_{n_f}^+ | 1_{n_i}^+ \rangle$  is [58]

$$\begin{aligned} \langle 1_{n_f}^+ | 1_{n_i}^+ \rangle &= \sum_{\pi_i \nu_i} \sum_{\pi_f \nu_f} C_{\pi_i \pi_f} C_{\nu_i \nu_f} (X_{\pi_i \nu_i}^{n_i} X_{\pi_f \nu_f}^{n_f} - Y_{\pi_i \nu_i}^{n_i} Y_{\pi_f \nu_f}^{n_f}) \\ &\times (u_{\pi_i} u_{\pi_f} + v_{\pi_i} v_{\pi_f}) (u_{\nu_i} u_{\nu_f} + v_{\nu_i} v_{\nu_f}) \\ &\times \langle \text{HFB}^{(f)} | \text{HFB}^{(i)} \rangle, \end{aligned} \quad (8)$$

where  $C_{\pi_i \pi_f} = \langle \pi_i | \pi_f \rangle$  and  $C_{\nu_i \nu_f} = \langle \nu_i | \nu_f \rangle$  are the overlaps of the canonical single-particle wave functions. In the canonical basis, the overlap of the HFB ground states of initial and final nuclei reads

$$\begin{aligned} \langle \text{HFB}^{(f)} | \text{HFB}^{(i)} \rangle &= \prod_{\pi_i \pi_f \nu_i \nu_f} (u_{\pi_i} u_{\pi_f} + v_{\pi_i} v_{\pi_f}) \\ &\times (u_{\nu_i} u_{\nu_f} + v_{\nu_i} v_{\nu_f}). \end{aligned} \quad (9)$$

The excitation energy of the intermediate nucleus in the denominator is

$$\begin{aligned} E_{\text{int.}}(n_i, n_f) &= \frac{1}{2} (E_{\text{int.}}^{n_i} + E_{\text{int.}}^{n_f}) \\ &= \frac{1}{2} [(\Omega^{n_i} + \lambda_{\pi}^{(i)} - \lambda_{\nu}^{(i)}) - (M_{\text{int.}} - M_i) - \Delta m_{\nu\pi} \\ &\quad + (\Omega^{n_f} - \lambda_{\pi}^{(f)} + \lambda_{\nu}^{(f)}) - (M_{\text{int.}} - M_f) + \Delta m_{\nu\pi}] \\ &= \frac{1}{2} [(\Omega^{n_i} + \lambda_{\pi}^{(i)} - \lambda_{\nu}^{(i)}) + (\Omega^{n_f} - \lambda_{\pi}^{(f)} + \lambda_{\nu}^{(f)}) \\ &\quad - (2M_{\text{int.}} - M_i - M_f)], \end{aligned} \quad (10)$$

where  $\lambda$  denotes the Fermi surface and  $\Delta m_{\nu\pi}$  is the mass difference between the neutron and the proton, i.e.,  $m_{\nu} - m_{\pi}$ .  $\Omega^{n_i}$  and  $\Omega^{n_f}$  are the eigenvalues of QRPA equations for mother and daughter nuclei, respectively. With the use of Eq. (10), nuclear masses are eventually not needed in the calculation of the NME in Eq. (5); only the energy with respect to the mother nucleus ( $\Omega^{n_i} + \lambda_{\pi}^{(i)} - \lambda_{\nu}^{(i)}$ ) and the energy with respect to the daughter nucleus ( $\Omega^{n_f} - \lambda_{\pi}^{(f)} + \lambda_{\nu}^{(f)}$ ) are needed, and are obtained from QRPA calculations. However, to calculate

the energy of intermediate nucleus  $E_{\text{int.}}(n_i, n_f)$  the experimental mass values from AME2020 [59] are used for the masses of the initial nucleus  $M_i$ , the intermediate nucleus  $M_{\text{int.}}$ , and the final nucleus  $M_f$ .

### III. NUMERICAL DETAILS

For the Skyrme HFB calculations, the SkO' interaction [60] is used for the mean-field calculation. For the pairing interaction, we adopt the surface density-dependent  $\delta$  force, whose strength is fixed to reproduce the experimental pairing gap obtained from the five-point formula of binding energies as stated above. We use different cutoffs to reduce the computation burden and obtain required accuracy. For the mean field, we use a smooth cutoff for the pairing window with a diffuseness parameter  $\mu$  of 0.1 MeV, and the cutoff on equivalent Hartree-Fock energy  $\varepsilon^{\text{HF}}$  is set to be 80.0 MeV. For the QRPA calculation, we use the canonical basis ( $|\pi\rangle$  and  $|\nu\rangle$ ) with occupation amplitudes ( $u$  and  $v$ ), which are obtained by performing canonical transformation on the quasiparticle states in HFB calculations. The  $\pi$ - $\nu$  configurations are selected under the criterion  $|u_{\pi} v_{\nu}| > 10^{-4}$  or  $|u_{\nu} v_{\pi}| > 10^{-4}$ , with the single-particle energies in canonical basis  $\varepsilon_{\pi(\nu)} < 60.0$  MeV. For the calculations of  $M_{\text{GT}}^{2\nu}$  of specific intermediate states, only the  $\pi$ - $\nu$  configurations with  $|X_{\pi\nu}^2 - Y_{\pi\nu}^2| > 10^{-6}$  are taken. The strengths of isovector proton-neutron pairing  $f_{\text{IV}}$  are fixed by tuning  $M_{\text{F}}^{2\nu}$  to vanish. But since it does not affect the Gamow-Teller  $2\nu\beta\beta$  matrix element  $M_{\text{GT}}^{2\nu}$ , we will not discuss it in present work.

### IV. RESULTS AND DISCUSSIONS

#### A. Systematic study on $M_{\text{GT}}^{2\nu}$

We start with systematic study of the evolution of  $2\nu\beta\beta$ -decay NMEs ( $M_{\text{GT}}^{2\nu}$ ) on the IS pairing strength for 11 nuclei which have been measured. Results are depicted in Fig. 1 and compared with compiled data from Ref. [3]. From the figure, all these  $M_{\text{GT}}^{2\nu}$  decrease when IS pairing strength is large enough. This suppression effect of IS pairing, as a common feature found in QRPA calculations, has been well analyzed in Refs. [26,61]. The decreasing behavior of the  $M_{\text{GT}}^{2\nu}$  with increasing IS pairing strength enables us to find the appropriate strength parameter  $f_{\text{IS}}$  to reproduce the experimental values, as listed in Table I. If one further increases the IS pairing strength, the  $M_{\text{GT}}^{2\nu}$  passes through zero and changes its sign. It has been found that the broken Wigner spin-isospin SU(4) symmetry is restored when the  $2\nu\beta\beta$  closure matrix element  $M_{\text{GTcl}}^{2\nu} = \langle f | \sum_{mn} \vec{\sigma}_m \cdot \vec{\sigma}_n \tau_m^+ \tau_n^+ | i \rangle = 0$  [27,30,33,34]. We note that besides the IS pairing the nuclear deformation also leads to the suppression of the  $M_{\text{GT}}^{2\nu}$  [29,58], mostly due to the difference between the shapes of initial and final nuclei, which will not be discussed in present work.

In Table I, we list the experimental and theoretical values of  $M_{\text{GT}}^{2\nu}$  for these 11 nuclei. The isoscalar pairing strength parameters  $f_{\text{IS}}$  used in QRPA calculations are listed in the last column. We observe that most of the determined  $f_{\text{IS}}$  are around 1.2, which means the ground-state correlation should be large enough to suppress the  $M_{\text{GT}}^{2\nu}$ . For the nuclei with magic numbers,  $^{48}\text{Ca}$ ,  $^{116}\text{Cd}$ , and  $^{136}\text{Xe}$ , their  $f_{\text{IS}}$  values are

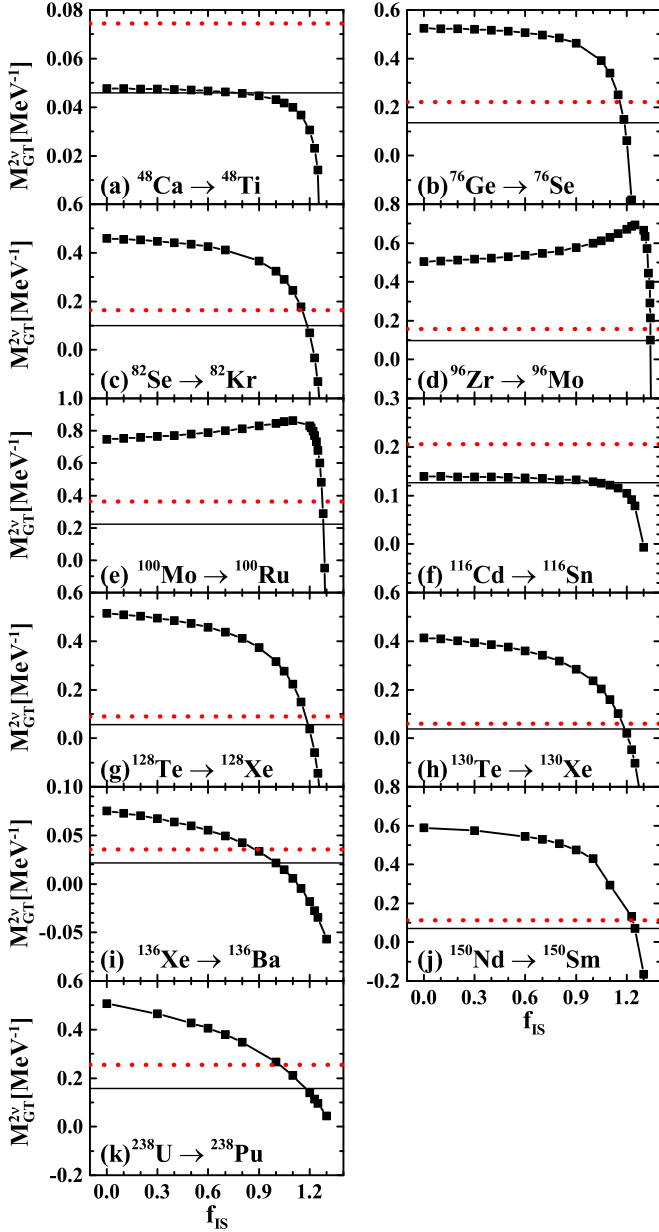


FIG. 1. The  $2\nu\beta\beta$  nuclear matrix elements  $M_{GT}^{2\nu}$  for 11 nuclei as a function of isocalar pairing strength parameter (black square). The horizontal lines represent the experimental values extracted from Ref. [3] with  $g_A = 1.00$  (red dotted) and  $g_A = 1.27$  (black dashed)

relatively small. This is probably caused by the overestimated small ground-state overlap factor due to the violation of particle number in the QRPA model [62], and this needs further investigation. We further examine the SSD and the extended LLD hypotheses, so the  $M_{GT}^{2\nu}$  obtained from the SSD or LLD hypothesis  $M_{GT}^{2\nu}$  (SSD or LLD) are also listed in Table I. When  $g_A = 1.27$  (bare value), for  $^{48}\text{Ca}$ ,  $^{82}\text{Se}$ ,  $^{116}\text{Cd}$ ,  $^{128}\text{Te}$ , and  $^{238}\text{U}$ , the first  $1^+$  states of the intermediate nuclei contribute more than 75% to the total NMEs. In this sense, the SSD hypothesis is fulfilled for these nuclei. On the other hand, when  $g_A = 1.00$  (quenched value), only  $^{238}\text{U}$  still fulfills the SSD hypothesis. The inconsistency on the evidence of SSD in  $^{100}\text{Mo}$

TABLE I. Experimental and theoretical  $2\nu\beta\beta$  nuclear matrix elements  $M_{GT}^{2\nu}$  for 11 nuclei in units of  $\text{MeV}^{-1}$ , when  $g_A = 1.27$  and  $g_A = 1.00$ .  $M_{GT}^{2\nu}$  obtained by the single-state dominance (SSD) and low-lying-states dominance (LLD) hypotheses are also listed. The upper limit of the energy for low-lying states  $E_{\text{int.}}$  in LLD is set as 5 MeV. The isocalar pairing strength parameters used in QRPA calculations are listed in the last column. The experimental values of  $M_{GT}^{2\nu}$  are taken from Ref. [3]. The results of  $^{48}\text{Ca}$  and  $^{116}\text{Cd}$  when  $g_A = 1.00$  are not listed, because the experimental NMEs are always larger than the theoretical ones with this value of  $g_A$ .

Nucleus	$g_A$	Expt. $M_{GT}^{2\nu}$	Theor. $M_{GT}^{2\nu}$	Theor. $M_{GT}^{2\nu}$ (SSD)	Theor. $M_{GT}^{2\nu}$ (LLD)	$f_{\text{IS}}$
$^{48}\text{Ca}$	1.27	$0.046 \pm 0.004$	0.046	0.036	0.036	0.7570
$^{76}\text{Ge}$	1.27	$0.137 \pm 0.007$	0.136	0.071	0.188	1.1852
	1.00	$0.221 \pm 0.012$	0.221	0.082	0.256	1.1612
$^{82}\text{Se}$	1.27	$0.101 \pm 0.005$	0.100	0.104	0.161	1.1886
	1.00	$0.162 \pm 0.008$	0.162	0.095	0.191	1.1594
$^{96}\text{Zr}$	1.27	$0.097 \pm 0.005$	0.099	0.351	0.252	1.3411
	1.00	$0.157 \pm 0.008$	0.158	0.405	0.309	1.3399
$^{100}\text{Mo}$	1.27	$0.224 \pm 0.006$	0.224	0.515	0.346	1.2824
	1.00	$0.362 \pm 0.010$	0.361	0.631	0.478	1.2768
$^{116}\text{Cd}$	1.27	$0.127 \pm 0.004$	0.127	0.112	0.124	1.0350
$^{128}\text{Te}$	1.27	$0.056 \pm 0.007$	0.057	0.043	0.113	1.1928
	1.00	$0.090 \pm 0.012$	0.091	0.047	0.130	1.1788
$^{130}\text{Te}$	1.27	$0.038 \pm 0.005$	0.037	0.020	0.087	1.1912
	1.00	$0.061 \pm 0.008$	0.062	0.022	0.095	1.1776
$^{136}\text{Xe}$	1.27	$0.022 \pm 0.001$	0.022	0.003	0.007	0.9968
	1.00	$0.035 \pm 0.001$	0.035	0.004	0.011	0.8820
$^{150}\text{Nd}$	1.27	$0.070 \pm 0.005$	0.070	0.240	0.257	1.2503
	1.00	$0.114 \pm 0.008$	0.116	0.246	0.289	1.2360
$^{238}\text{U}$	1.27	$0.158^{+0.109}_{-0.085}$	0.157	0.185	0.185	1.1787
	1.00	$0.254^{+0.176}_{-0.137}$	0.254	0.230	0.230	1.0251

reported in Refs. [16,17] could be the nuclear deformation that is not included in our model [14]. We further test the LLD hypothesis for the nuclei whose NMEs do not fulfill the SSD hypothesis. Because there is not a definite upper limit of the energy for low-lying states in intermediate nuclei, we set it as 5 MeV. When  $g_A = 1.00$ , these low-lying states contribute almost the full NMEs for  $^{76}\text{Ge}$  and  $^{82}\text{Se}$ . In this sense, the NMEs for these nuclei fulfill the LLD hypothesis.

In Fig. 2, with the determined  $f_{\text{IS}}$  in Table I, the running sums of  $M_{GT}^{2\nu}$  for these 11 nuclei are depicted. The results of  $g_A = 0.80$  are also shown, since this value of  $g_A$  has been used in Ref. [63]. Generally, the behaviors of running sums can be divided into three types when  $g_A = 1.27$ . The first one is steadily increasing accompanied with small fluctuations, as shown in  $^{48}\text{Ca}$  and  $^{116}\text{Cd}$ . The second type is that the contributions from first few lowest states are large enough but then the following excited states give continuous negative contributions, and hence provide a suppression due to the cancellation between lowest states and higher-lying states, as in  $^{96}\text{Zr}$ ,  $^{100}\text{Mo}$ , or  $^{150}\text{Nd}$ . The last type is the most common one, observed in 6 of total 11 nuclei, i.e.,  $^{76}\text{Ge}$ ,  $^{82}\text{Se}$ ,  $^{128}\text{Te}$ ,  $^{130}\text{Te}$ ,  $^{136}\text{Xe}$ , and  $^{238}\text{U}$ . The cumulative contributions continuously increase up to the excitation energy of the intermediate nucleus  $E_{\text{int.}}$  around 10 MeV (for  $^{136}\text{Xe}$  and  $^{238}\text{U}$ ,



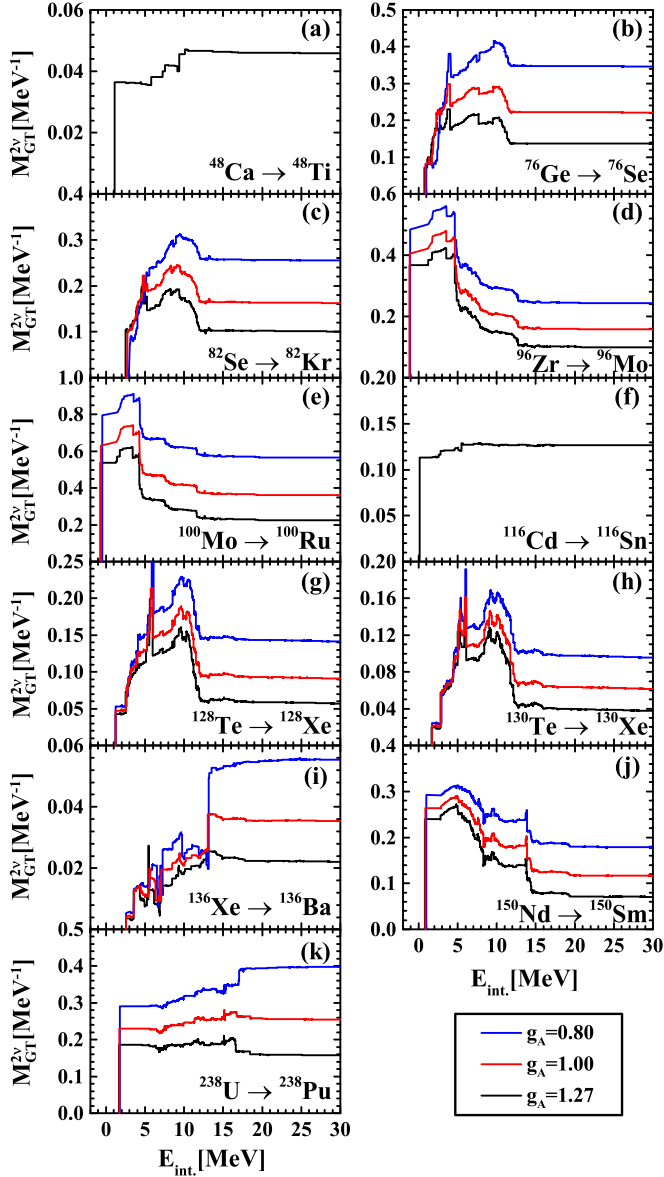


FIG. 2. Running sums of  $M_{GT}^{2\nu}$  for 11 nuclei as a function of the excitation energy of the intermediate nucleus with  $g_A = 0.80$  (blue),  $g_A = 1.00$  (red), and  $g_A = 1.27$  (black). The IS pairing strength parameters  $f_{IS}$  used for the corresponding calculations are also shown in the figure.

it is 15 MeV), then a remarkable cancellation appears due to the negative contributions of higher-lying states, similarly to the case of the second type. The difference between the second and third types is how the medium energy states with 5–10 MeV contribute. The cancellation between positive contributions from the low-lying states and negative contributions from the higher-lying states leads to the realization of SSD for  $^{82}\text{Se}$  and  $^{128}\text{Te}$  when  $g_A = 1.27$ , and LLD for  $^{76}\text{Ge}$  and  $^{82}\text{Se}$  when  $g_A = 1.00$ . The negative contributions in the running sums seem to be universal, and also appear in the results calculated by the shell model with complete spin-orbit partner model space [25,64] and QRPA models [23,24,42,43]. Compared to the nuclei of the second and third types, it is noticed

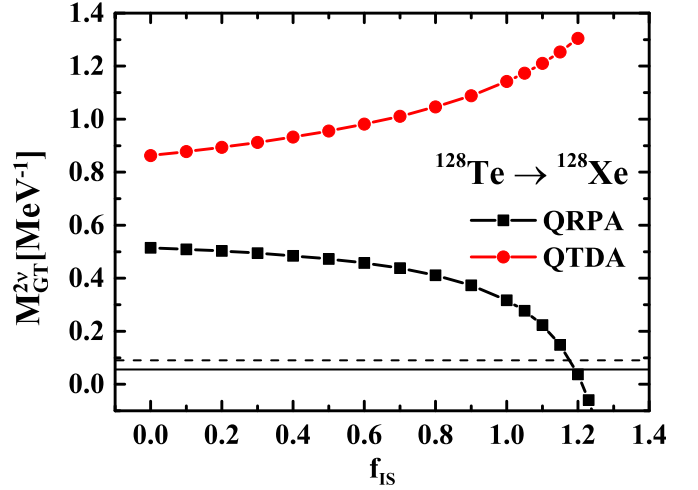


FIG. 3. The  $2\nu\beta\beta$  nuclear matrix elements  $M_{GT}^{2\nu}$  for  $^{128}\text{Te}$  as a function of isoscalar pairing strength parameter calculated by QRPA (black square) and QTDA (red circle). The horizontal lines represent the experimental values with  $g_A = 1.27$  (solid) and  $g_A = 1.00$  (dashed).

that the IS pairing strength parameters  $f_{IS}$  are smaller for the nuclei of the first type. On the other hand, from Fig. 1, when increasing  $g_A$ , the strength of proton-neutron isoscalar pairing  $f_{IS}$  should also be increased to reproduce the experimental NME. By comparing the running sums of  $g_A = 0.80$ , 1.00 and 1.27, one can find that when  $g_A$  is increasing the negative contributions can either be induced, e.g., in  $^{136}\text{Xe}$  and  $^{238}\text{U}$ , or be enlarged, e.g., in  $^{82}\text{Se}$ ,  $^{128}\text{Te}$ , and  $^{130}\text{Te}$ . Therefore, these two aspects indicate that the appearance of negative contributions in the running sums are closely related to the magnitude of  $f_{IS}$ , which controls the amount of ground-state correlations introduced in QRPA [24]. So, without losing generality, we will pick  $^{128}\text{Te}$  as an example and analyze the mechanism for the negative contributions of high-lying states at large  $f_{IS}$  in the next subsections.

### B. Ground-state correlations: QRPA versus QTDA

As stated above, the negative contributions in the running sums are related to the ground-state correlations in the QRPA model. In this subsection, to analyze the effects of the ground-state correlations, as an example, we compare the QRPA model and the QTDA (quasiparticle Tamm-Dancoff approximation) model calculations of the  $M_{GT}^{2\nu}$  for  $^{128}\text{Te}$ . Unlike the QRPA model, the ground state of the QTDA model is the quasiparticle vacuum with no ground-state correlation, that is without the backward amplitude  $Y_{\pi\nu}$  term. In Fig. 3, the evolutions of  $M_{GT}^{2\nu}$  as a function of IS pairing strength  $f_{IS}$  from QRPA and QTDA models are shown. These two results are different from each other. The  $M_{GT}^{2\nu}$  calculated by QTDA model monotonically increases with increasing  $f_{IS}$  and is systematically larger than that from the QRPA model. The latter shows explicitly the suppression effect from the ground-state correlations. This is consistent with the conclusion of Ref. [28].

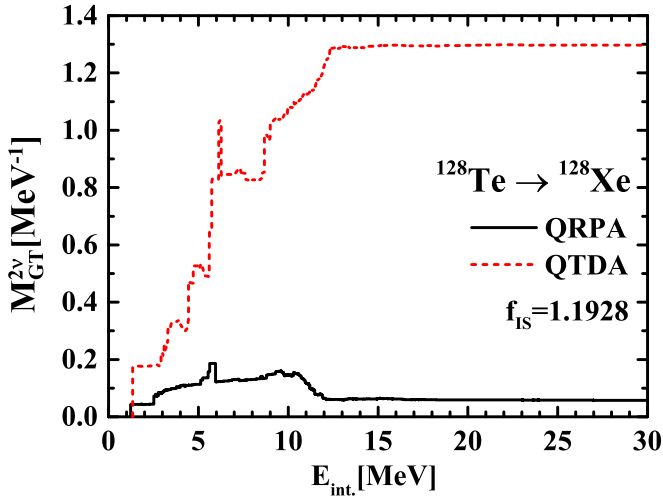


FIG. 4. Running sums of the  $M_{GT}^{2\nu}$  for  $^{128}\text{Te}$  as a function of the excitation energy of the intermediate nucleus calculated by QRPA (black solid line) and QTDA (red dashed line) with the isoscalar pairing strength parameter  $f_{IS} = 1.1928$ .

In Fig. 4 we show the running sums of  $M_{GT}^{2\nu}$  calculated by the QTDA model and the QRPA model with  $f_{IS} = 1.1928$ , with which value of  $f_{IS}$  the experimental NME of  $^{128}\text{Te}$  can be reproduced by the QRPA model. One finds that in the region of  $E_{int.} < 9.0$  MeV the running sums of these two models are different in magnitude but evolve similarly. However, in the region of  $9.0 < E_{int.} < 12.0$  MeV, the running sum of the QTDA model keeps increasing, while that of the QRPA model starts to decrease. Therefore, the negative contributions of high-lying states are related to the ground-state correlations introduced in the QRPA model. Finally, running sum curves of both models become flat after  $E_{int.}$  equals about 12.0 MeV around the GT resonance (GTR) region, because of large energy denominators and small transition amplitudes for these very highly excited states beyond GTR.

To understand the large difference between the  $M_{GT}^{2\nu}$  calculated by QRPA and QTDA models, we further investigate  $GT^-$  and  $GT^+$  transition branches involved in the calculation of  $M_{GT}^{2\nu}$  as shown in Eq. (5). The corresponding transition strengths  $S(GT^-)$  and  $S(GT^+)$  are shown in Fig. 5. Since  $^{128}\text{Te}$  has excess neutrons, its  $GT^-$  transition strength is large, so the inclusion of  $Y_{\pi\nu}$  amplitude in the QRPA calculation does not make it different from the QTDA calculation without the  $Y_{\pi\nu}$  term. However, the  $GT^+$  transition strength of  $^{128}\text{Xe}$  is small, due to the blocking effects of the Pauli principle with large neutron excess. The inclusion of ground-state isovector pairing correlations could unblock some transition channels and increase the  $GT^+$  transition strength. The inclusion of the backward amplitude  $Y_{\pi\nu}$ , the ground-state correlations introduced in the QRPA model, have also significant influence on the  $GT^+$  transition strength through the relatively big  $u_{\pi\nu}v_{\nu}$  factor in front of  $Y_{\pi\nu}$ . Due to the opposite signs of  $X_{\pi\nu}$  and  $Y_{\pi\nu}$ , for  $^{128}\text{Xe}$  the  $GT^+$  transition strength becomes smaller in the QRPA calculation compared to that of the QTDA calculation. Through the above comparison, it is clear that the ground-state correlations, namely the large backward amplitudes  $Y_{\pi\nu}$  in

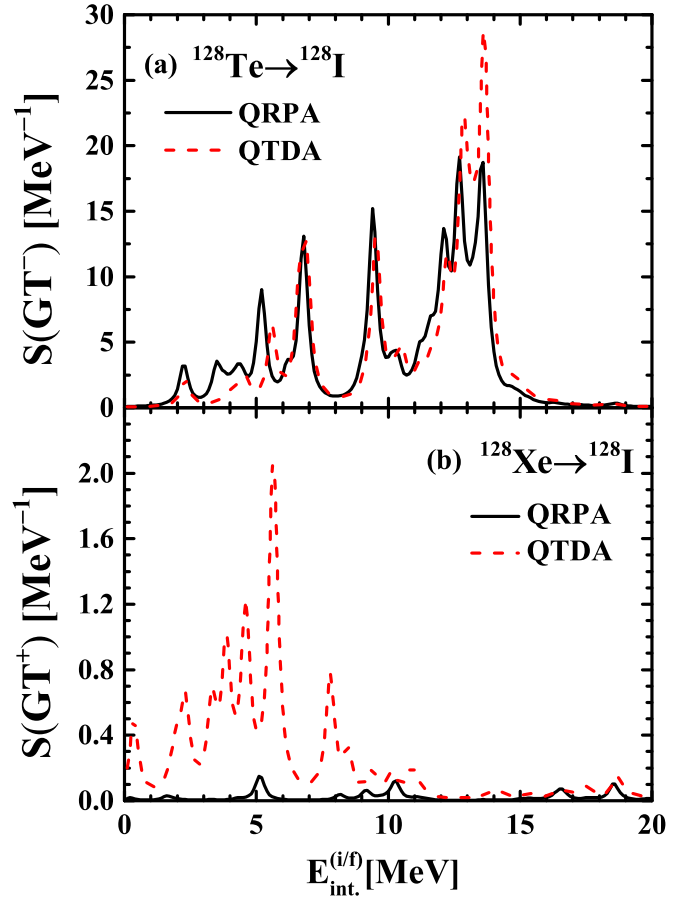


FIG. 5. The  $GT^-$  transition strength function of  $^{128}\text{Te} \rightarrow ^{128}\text{I}$  whose excitation energies  $E_{int.}^{(i)}$  are with respect to  $^{128}\text{I}$  (a) and  $GT^+$  transition strength function of  $^{128}\text{Xe} \rightarrow ^{128}\text{I}$  whose excitation energies  $E_{int.}^{(f)}$  are with respect to  $^{128}\text{I}$  (b). The black solid lines and red dashed lines are the results calculated by QRPA and QTDA, respectively.

QRPA induced by strong IS pairing, play crucial roles in the calculation of  $M_{GT}^{2\nu}$  through their effects on the  $GT^+$  transition of the daughter nucleus.

### C. Negative contributions in running sum

By comparing running sums of the QRPA model and the QTDA model in Sec. IV B, we come to the conclusion that the negative contributions are related to ground-state correlations introduced by the  $Y_{\pi\nu}$  term which can be enhanced by large IS pairing. Actually, there is a close relation between IS pairing and ground-state correlations introduced by the  $Y_{\pi\nu}$  term. With the increase of IS pairing strength, the magnitude of  $B$  matrix elements in QRPA equation (2b) increases as well due to the attractive nature of IS pairing residual interaction. As a result, the  $Y_{\pi\nu}$  amplitude will increase, as also explained in Ref. [26]. We depict the running sums of the  $M_{GT}^{2\nu}$  for  $^{128}\text{Te}$  with different  $f_{IS}$  and  $\eta_Y$  in Fig. 6. From the figure, the behaviors of the running sum curves are very similar when increasing  $f_{IS}$  and  $\eta_Y$ . Especially, in both cases the negative contributions will be induced and further be enlarged in the 9–15 MeV region (around the GTR). Based on such a relation, to simulate the

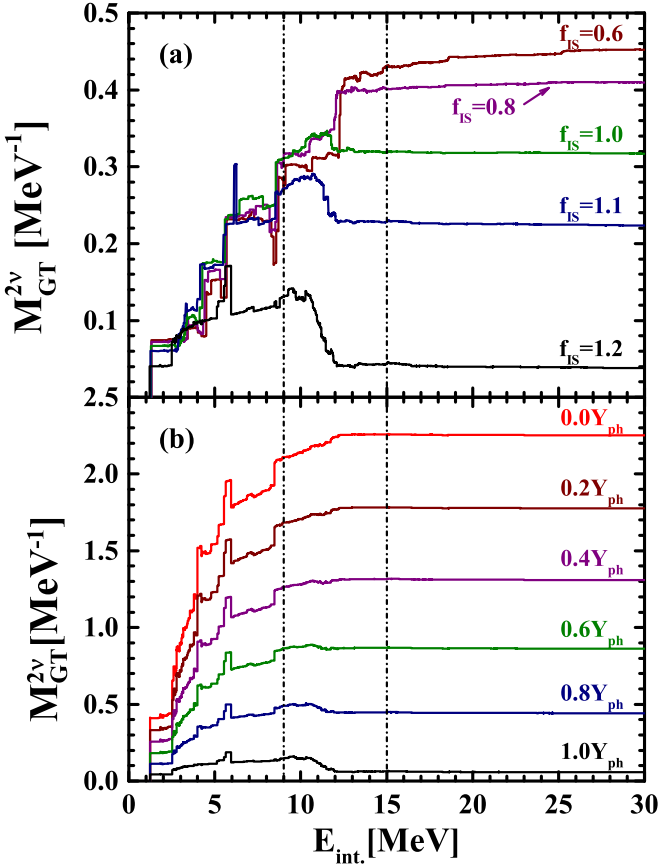


FIG. 6. Running sums of the  $M_{GT}^{2v}$  for  $^{128}\text{Te}$  with different  $f_{IS}$  (a) and  $\eta_Y$  (b) as a function of the excitation energy of the intermediate nucleus.

increase of the IS pairing strength, we change the magnitude of  $Y_{\pi\nu}$  by replacing it with  $\eta_Y Y_{\pi\nu}$  in the calculation of transition amplitudes, where the factor  $\eta_Y$  varies from 0.0 to 1.0. The purpose of this study is to understand how negative contributions to  $M_{GT}^{2v}$  happen at large IS pairing strength. One of the advantages of such a simulation, instead of varying the IS pairing strength directly, is that one can avoid the complicated splittings and degeneracy in the excited spectra caused by the variation of the IS pairing.

The trend of the results with  $\eta_Y = 0.0$  is very similar to that of the QTDA model in Fig. 4. With the increasing  $\eta_Y$ , two features of the running sum curves are emerging. The first one is that the contributions from the region  $E_{\text{int.}} < 9.0$  MeV decrease significantly. The second one is that the majority of these contributions in the region of  $9.0 < E_{\text{int.}} < 15.0$  MeV change their signs from positive to negative values. It can be seen that negative contributions do appear with large enough  $Y_{\pi\nu}$  amplitudes in our simulation. Then what is the origin of these negative contributions? To answer this question, in Fig. 7, we explicitly show the contributions to  $M_{GT}^{2v}$  of intermediate states with excitation energy ranging from 9.0 to 15.0 MeV as a function of  $\eta_Y$ . The total contribution (black square) decreases monotonically from positive to negative values. Then we separate the contributions which have changes in sign for the increasing  $\eta_Y$ , denoted as  $M_{GT}^{\prime 2v}$  (red circle). From

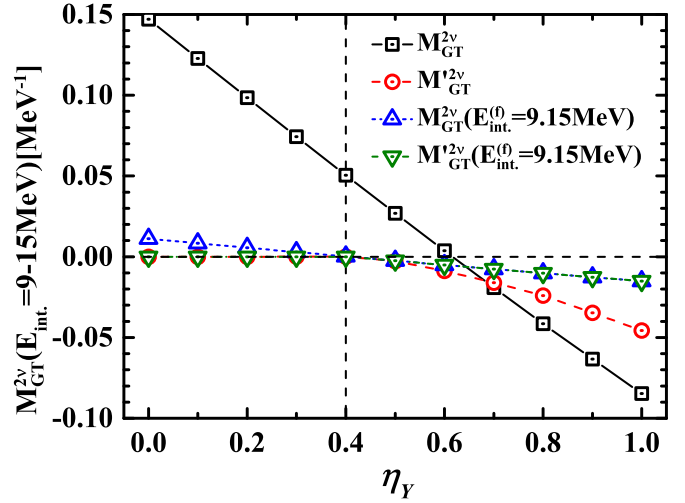


FIG. 7. Contributions to  $M_{GT}^{2v}$  for  $^{128}\text{Te}$  from excitation energies of the intermediate nucleus ranging 9.0–15.0 MeV. Black square: the total contribution of all intermediate states in the 9.0–15.0 MeV excitation energy region. Red circle: sum of the contributions whose signs have changed relative to  $\eta_Y = 0.0$  during increase of  $\eta_Y$ . Blue up triangle: sum of the contributions of those intermediate states with one coming from  $\text{GT}^+$  transition of the daughter nucleus with an excitation energy of  $E_{\text{int.}}^{(f)} = 9.15$  MeV. Green down triangle: sum of the contributions with  $E_{\text{int.}}^{(f)} = 9.15$  MeV whose signs have changed relative to  $\eta_Y = 0.0$  during increase of  $\eta_Y$ .

the figure, we observe that the  $M_{GT}^{\prime 2v}$  contributes remarkably more than 50% to the  $M_{GT}^{2v}$  at  $\eta_Y = 1.0$ . So a main reason that the negative contributions appear is the change of signs of  $M_{GT}^{2v}$  contributed by some intermediate states. Among these intermediate states, one non-negligible contribution comes from those with an excitation energy of  $E_{\text{int.}}^{(f)} = 9.15$  MeV from the  $\text{GT}^+$  transition side of the daughter nucleus. We note that the rest of the negative contributions do not change their signs with increasing  $\eta_Y$ , but they are small at  $\eta_Y = 0.0$  and become large at  $\eta_Y = 1.0$ .

To get a deeper insight for these sign changes, we investigate the  $\text{GT}^-$  and  $\text{GT}^+$  transitions. From Eq. (5), the  $M_{GT}^{2v}$  for a specific intermediate state is proportional to the  $\text{GT}^-$  transition amplitude  $\langle 1_{\text{int.}}^+ || \text{GT}^- || 0_{\text{g.s.}}^{+(i)} \rangle$  and the  $\text{GT}^+$  transition amplitude  $\langle 1_{\text{int.}}^+ || \text{GT}^+ || 0_{\text{g.s.}}^{+(f)} \rangle$ . So we pick several typical  $\text{GT}^-$  and  $\text{GT}^+$  states with excitation energies in the range of  $E_{\text{int.}} < 9.0$  MeV and in the range of  $9.0 < E_{\text{int.}} < 15.0$  MeV, and plot their transition amplitudes as a function of  $\eta_Y$  in Fig. 8. These six typical states are chosen for the following reasons: The states at  $E_{\text{int.}}^{(i)} = 2.25$  MeV and  $E_{\text{int.}}^{(f)} = 0.21$  MeV are the first  $1^+$  states calculated from  $^{128}\text{Te}$  and  $^{128}\text{Xe}$ , respectively. The state at  $E_{\text{int.}}^{(f)} = 5.14$  MeV has the largest  $\text{GT}^+$  transition amplitude in the 0–9.0 MeV region. For this state, the largest overlap factor  $\langle 1_{n_f}^+ | 1_{n_i}^+ \rangle$  is produced by the state at  $E_{\text{int.}}^{(i)} = 6.17$  MeV. The state at  $E_{\text{int.}}^{(f)} = 9.15$  MeV has the largest  $\text{GT}^+$  transition amplitude (absolute value) among the states whose  $\text{GT}^+$  transition amplitudes have changed their signs in the 9.0–15.0 MeV region. For this state, the largest overlap factor  $\langle 1_{n_f}^+ | 1_{n_i}^+ \rangle$  produced by the state lying in

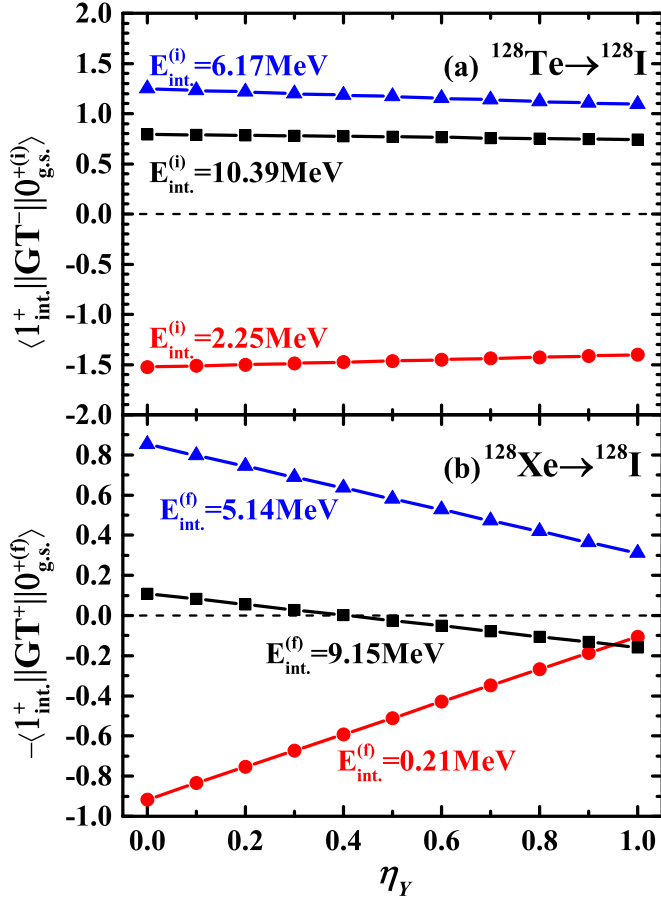


FIG. 8. The  $\text{GT}^-$  transition amplitudes for three excited states in  $^{128}\text{Te}$  (a) and  $\text{GT}^+$  transition amplitudes for three excited states in  $^{128}\text{Xe}$  (b) as a function of  $\eta_Y$ . The values of excitation energies relative to  $^{128}\text{I}$  are shown in the figure.

9.0–15.0 MeV is the state at  $E_{\text{int.}}^{(i)} = 10.39$  MeV. From Fig. 8(a), we find that the  $\text{GT}^-$  transition amplitudes are almost independent of  $\eta_Y$ , which is consistent with  $B(\text{GT}^-)$  being little influenced by the IS pairing. On the other hand, the  $\text{GT}^+$  transition amplitudes, in panel (b), show a strong dependence on  $\eta_Y$ , and even change their signs for the higher excited states with  $E_{\text{int.}}^{(f)} = 9.15$  MeV. Such a strong dependence comes from the large magnitude of the  $u_{\pi}v_{\nu}$  factor in front of  $Y_{\pi\nu}$  for neutron-rich nuclei. For the  $\text{GT}^+$  state of  $E_{\text{int.}}^{(f)} = 9.15$  MeV, one can observe that after  $\eta_Y = 0.4$  the  $\text{GT}^+$  transition amplitude crosses zero. Therefore, the summed contribution, coming from the  $(n_i, n_f)$  intermediate states with  $\text{GT}^+$  state of  $E_{\text{int.}}^{(f)} = 9.15$  MeV, change their signs and become negative, as shown by the blue up triangle in Fig. 7. On the other hand, for the  $\text{GT}^+$  states with energies smaller than 9.0 MeV, such as those with  $E_{\text{int.}}^{(f)} = 0.21$  or 5.14 MeV shown in the figure, the absolute values of their transition amplitudes keep decreasing with increasing  $\eta_Y$ , which causes the first feature observed in Fig. 6. Therefore, the variation of the  $\text{GT}^+$  transition amplitudes with  $\eta_Y$  for different energy regions of  $E_{\text{int.}}$  gives rise to the two features in Fig. 6

mentioned above. These two features are different because the  $\text{GT}^+$  transitions are unblocked by pairing correlation for low-lying states with energies smaller than 9.0 MeV, and hence there are non-negligible transition strengths in the case of  $\eta_Y = 0.0$ . The increase of  $\eta_Y$  can greatly reduce the  $\text{GT}^+$  transition amplitudes in this energy region, but is not enough to change their signs. On the other hand, for high-lying states with energies larger than 9.0 MeV, the  $\text{GT}^+$  transitions are almost blocked and have small strengths at  $\eta_Y = 0.0$ . In this case, the sign of  $\text{GT}^+$  transition amplitude can be changed easily due to the increase of  $Y_{\pi\nu}$  amplitude. At the end, we conclude that it is the enhanced ground-state correlations tuned by strong IS pairing interaction that cause the negative contributions to  $M_{\text{GT}}^{2\nu}$  in the energy range of 9.0–15.0 MeV, through their influence on the  $\text{GT}^+$  transition amplitudes.

## V. SUMMARY

In summary, we study the  $2\nu\beta\beta$ -decay nuclear matrix elements  $M_{\text{GT}}^{2\nu}$  based on the spherical Skyrme HFB + QRPA model, for 11 nuclei with experimental data, and the underlying mechanism for the fulfillment of the SSD or LLD hypothesis is revealed.

In our systematic investigation of  $M_{\text{GT}}^{2\nu}$ , the suppression effect of the IS pairing is found. By using the IS pairing strength determined through reproducing the experimental data with different axial-vector coupling constants  $g_A$ , we investigate the SSD and LLD hypotheses. When  $g_A = 1.27$ , the SSD hypothesis is fulfilled by the NMEs of  $^{48}\text{Ca}$ ,  $^{82}\text{Se}$ ,  $^{116}\text{Cd}$ ,  $^{128}\text{Te}$ , and  $^{238}\text{U}$ . When  $g_A = 1.00$ , the SSD hypothesis is fulfilled by the NMEs of  $^{238}\text{U}$ , while the LLD hypothesis is fulfilled by the NMEs of  $^{76}\text{Ge}$ , and  $^{82}\text{Se}$ . The realization of SSD and LLD hypotheses for  $^{76}\text{Ge}$ ,  $^{82}\text{Se}$  and  $^{128}\text{Te}$  are to a large extent caused by the negative contributions in the running sums of the NMEs. Through the comparison of the running sums of different  $g_A$ , we find that by increasing  $g_A$ , or alternatively  $f_{\text{IS}}$ , the negative contributions can either be induced or enlarged.

We pick  $^{128}\text{Te}$  as an example to further study the reason for these negative contributions in the running sum. By comparing the running sums of QRPA and QTDA models, the negative contributions are found to be related to the strong ground-state correlations induced by large IS pairing strength, which shows the importance of QRPA calculations over the simpler QTDA calculations for NME of  $2\nu\beta\beta$  decay. Through the study of  $\text{GT}^-$  and  $\text{GT}^+$  transition strength functions, it is shown that the ground-state correlations influence the NME through its crucial role in  $\text{GT}^+$  transitions for these double- $\beta$  decay nuclei with neutron excess, where many  $\text{GT}^+$  transition channels are blocked because of the Pauli principle.

With the inclusion of ground-state correlations in QRPA calculations, the increase of IS pairing strength will make their contributions larger so that they lead to the suppression of NME contributed from the energy region of intermediate states  $E_{\text{int.}} < 9.0$  MeV as well as negative contributions from  $9.0 < E_{\text{int.}} < 15.0$  MeV. Ground-state correlations play their roles on the above two features by suppressing  $\text{GT}^+$  transition



amplitudes of low-lying states and changing the signs of  $GT^+$  transition amplitudes of higher-lying states.

### ACKNOWLEDGMENTS

Y.F.N. and W.L.L. acknowledge the support of the National Natural Science Foundation of China under Grant

No. 12075104, and the Fundamental Research Funds for the Central Universities under Grant No. Izujbky-2021-it10. D.L.F. acknowledges the support of the “Light of West” program and the “from zero to one” program by CAS. C.L.B. acknowledges the support of the National Natural Science Foundation of China under Grants No. 11575120 and No. 11822504.

- 
- [1] M. Goepfert-Mayer, *Phys. Rev.* **48**, 512 (1935).  
 [2] S. R. Elliott, A. A. Hahn, and M. K. Moe, *Phys. Rev. Lett.* **59**, 2020 (1987).  
 [3] A. Barabash, *Nucl. Phys. A* **935**, 52 (2015).  
 [4] W. Haxton and G. Stephenson, *Prog. Part. Nucl. Phys.* **12**, 409 (1984).  
 [5] F. T. Avignone, S. R. Elliott, and J. Engel, *Rev. Mod. Phys.* **80**, 481 (2008).  
 [6] A. Faessler and F. Šimkovic, *J. Phys. G: Nucl. Part. Phys.* **24**, 2139 (1998).  
 [7] J. Suhonen and O. Civitarese, *Phys. Rep.* **300**, 123 (1998).  
 [8] J. Engel and J. Menéndez, *Rep. Prog. Phys.* **80**, 046301 (2017).  
 [9] H. Ejiri, J. Suhonen, and K. Zuber, *Phys. Rep.* **797**, 1 (2019).  
 [10] J. M. Yao, J. Meng, Y. F. Niu, and P. Ring, *arXiv:2111.15543*.  
 [11] J. Kotila and F. Iachello, *Phys. Rev. C* **85**, 034316 (2012).  
 [12] S. Stoica and M. Mirea, *Phys. Rev. C* **88**, 037303 (2013).  
 [13] J. Abad, A. Morales, R. Nunez-Lagos, and A. F. Pacheco, *Ann. Fis. A* **80**, 9 (1984).  
 [14] O. Moreno, R. Álvarez-Rodríguez, P. Sarriguren, E. Moya de Guerra, F. Šimkovic, and A. Faessler, *J. Phys. G: Nucl. Part. Phys.* **36**, 015106 (2008).  
 [15] O. Azzolini, J.W. Beeman, F. Bellini, M. Beretta, M. Biassoni, C. Brofferio, C. Bucci, S. Capelli, L. Cardani, P. Carniti, N. Casali, D. Chiesa, M. Clemenza, O. Cremonesi, A. Cruciani, I. Dafinei, S. DiDomizio, F. Ferroni, L. Gironi, A. Giuliani *et al.*, *Phys. Rev. Lett.* **123**, 262501 (2019).  
 [16] E. Armengaud, C. Augier, A. Barabash *et al.*, *Eur. Phys. J. C* **80**, 674 (2020).  
 [17] R. Arnold, C. Augier, A. S. Barabash *et al.*, *Eur. Phys. J. C* **79**, 440 (2019).  
 [18] O. Civitarese and J. Suhonen, *Phys. Rev. C* **58**, 1535 (1998).  
 [19] O. Civitarese and J. Suhonen, *Nucl. Phys. A* **653**, 321 (1999).  
 [20] F. Šimkovic, P. Domin, and S. V. Semenov, *J. Phys. G: Nucl. Part. Phys.* **27**, 2233 (2001).  
 [21] P. Domin, S. Kovalenko, F. Šimkovic, and S. Semenov, *Nucl. Phys. A* **753**, 337 (2005).  
 [22] P. Sarriguren, O. Moreno, and E. Moya de Guerra, *Adv. High Energy Phys.* **2016**, 6391052 (2016).  
 [23] F. Šimkovic, A. Smetana, and P. Vogel, *Phys. Rev. C* **98**, 064325 (2018).  
 [24] D. Fang, A. Faessler, V. Rodin, M. S. Yousef, and F. Šimkovic, *Phys. Rev. C* **81**, 037303 (2010).  
 [25] M. Horoi, S. Stoica, and B. A. Brown, *Phys. Rev. C* **75**, 034303 (2007).  
 [26] P. Vogel and M. R. Zirnbauer, *Phys. Rev. Lett.* **57**, 3148 (1986).  
 [27] V. Rodin and A. Faessler, *Phys. Rev. C* **84**, 014322 (2011).  
 [28] K. Muto, E. Bender, and H. V. Klapdor, *Z. Phys. A: Atom. Nucl.* **334**, 177 (1989).  
 [29] R. Álvarez-Rodríguez, P. Sarriguren, E. Moya de Guerra, L. Paceaescu, A. Faessler, and F. Šimkovic, *Phys. Rev. C* **70**, 064309 (2004).  
 [30] O. Civitarese and J. Suhonen, *Phys. Lett. B* **482**, 368 (2000).  
 [31] J. Suhonen, *Phys. Lett. B* **607**, 87 (2005).  
 [32] F. Šimkovic, V. Rodin, A. Faessler, and P. Vogel, *Phys. Rev. C* **87**, 045501 (2013).  
 [33] O. Rumyantsev and M. Urin, *Phys. Lett. B* **443**, 51 (1998).  
 [34] V. A. Rodin, M. H. Urin, and A. Faessler, *Nucl. Phys. A* **747**, 295 (2005).  
 [35] E. Caurier, F. Nowacki, and A. Poves, *Phys. Lett. B* **711**, 62 (2012).  
 [36] R. A. Sen'kov and M. Horoi, *Phys. Rev. C* **90**, 051301(R) (2014).  
 [37] B. A. Brown, D. L. Fang, and M. Horoi, *Phys. Rev. C* **92**, 041301(R) (2015).  
 [38] H. Li and Z. Ren, *Phys. Rev. C* **96**, 065503 (2017).  
 [39] L. Coraggio, L. De Angelis, T. Fukui, A. Gargano, N. Itaco, and F. Nowacki, *Phys. Rev. C* **100**, 014316 (2019).  
 [40] J. Suhonen, *Phys. Rev. C* **86**, 024301 (2012).  
 [41] P. Sarriguren, *Phys. Rev. C* **86**, 034335 (2012).  
 [42] J. Suhonen and O. Civitarese, *Nucl. Phys. A* **924**, 1 (2014).  
 [43] D. S. Delion and J. Suhonen, *Phys. Rev. C* **91**, 054329 (2015).  
 [44] D. Navas-Nicolás and P. Sarriguren, *Phys. Rev. C* **91**, 024317 (2015).  
 [45] F. Šimkovic, R. Dvornický, D. Štefánik, and A. Faessler, *Phys. Rev. C* **97**, 034315 (2018).  
 [46] J. Terasaki and Y. Iwata, *Phys. Rev. C* **100**, 034325 (2019).  
 [47] B. M. Dixit, P. K. Rath, and P. K. Raina, *Phys. Rev. C* **65**, 034311 (2002).  
 [48] R. Chandra, J. Singh, P. K. Rath, P. K. Raina, and J. G. Hirsch, *Eur. Phys. J. A* **23**, 223 (2005).  
 [49] S. Singh, R. Chandra, P. K. Rath, P. K. Raina, and J. G. Hirsch, *Eur. Phys. J. A* **33**, 375 (2007).  
 [50] P. K. Rath, R. Chandra, S. Singh, P. K. Raina, and J. G. Hirsch, *J. Phys. G: Nucl. Part. Phys.* **37**, 055108 (2010).  
 [51] P. K. Rath, R. Chandra, K. Chaturvedi, and P. K. Raina, *Front. Phys.* **7**, 64 (2019).  
 [52] N. Yoshida and F. Iachello, *Prog. Theor. Exp. Phys.* **2013**, 043D01 (2013).  
 [53] J. Barea, J. Kotila, and F. Iachello, *Phys. Rev. C* **91**, 034304 (2015).  
 [54] J. Dobaczewski, H. Flocard, and J. Treiner, *Nucl. Phys. A* **422**, 103 (1984).  
 [55] J. Dobaczewski, W. Nazarewicz, T. R. Werner, J. F. Berger, C. R. Chinn, and J. Dechargé, *Phys. Rev. C* **53**, 2809 (1996).

- [56] K. Bennaceur and J. Dobaczewski, *Comput. Phys. Commun.* **168**, 96 (2005).
- [57] H. Sagawa, C. L. Bai, and G. Colò, *Phys. Scr.* **91**, 083011 (2016).
- [58] F. Šimkovic, L. Paceaescu, and A. Faessler, *Nucl. Phys. A* **733**, 321 (2004).
- [59] W. Huang, M. Wang, F. Kondev, G. Audi, and S. Naimi, *Chin. Phys. C* **45**, 030002 (2021).
- [60] P.-G. Reinhard, D. J. Dean, W. Nazarewicz, J. Dobaczewski, J. A. Maruhn, and M. R. Strayer, *Phys. Rev. C* **60**, 014316 (1999).
- [61] O. Civitarese, A. Faessler, and T. Tomoda, *Phys. Lett. B* **194**, 11 (1987).
- [62] J. M. Yao, L. S. Song, K. Hagino, P. Ring, and J. Meng, *Phys. Rev. C* **91**, 024316 (2015).
- [63] A. Gando, Y. Gando, T. Hachiya, M. Ha Minh, S. Hayashida, Y. Honda, K. Hosokawa, H. Ikeda, K. Inoue, K. Ishidoshiro, Y. Kamei, K. Kamizawa, T. Kinoshita, M. Koga, S. Matsuda, T. Mitsui, K. Nakamura, A. Ono, N. Ota, S. Otsuka, and F. Šimkovic (KamLAND-Zen Collaboration), *Phys. Rev. Lett.* **122**, 192501 (2019).
- [64] H. Nakada, T. Sebe, and K. Muto, *Nucl. Phys. A* **607**, 235 (1996).